Supplemental Material

Rashba effect modulation in two-dimensional $A_2B_2Te_6$ (A = Sb, Bi; B = Si, Ge) materials via charge transfer

Haipeng Wu[1], Qikun Tian[2], Jinghui Wei[1], Ziyu Xing[1], Guangzhao Qin[2], Zhenzhen Qin[1*]

[1]*Key Laboratory of Materials Physics, Ministry of Education, School of Physics, Zhengzhou University, Zhengzhou 450001, P. R. China*

[2]*State Key Laboratory of Advanced Design and Manufacturing Technology for Vehicle, College of Mechanical and Vehicle Engineering, Hunan University, Changsha 410082, P. R. China*

[*] Corresponding author: qzz@zzu.edu.cn

Structural parameters of original and Janus monolayers

Table SI shows the optimized lattice parameters of original and Janus structures, the lattice parameters of the T-Janus $A_2B_2X_3Y_3$ monolayers range from 6.59 to 7.15 Å, where the $Bi_2Ge_2Se_3Te_3$ monolayer having the maximum lattice parameter of 7.15 Å; The lattice parameters of the I-Janus A_2BCX_6 monolayers range from 6.49 to 7.36 Å, where the $Bi_2SiGeTe_6$ monolayer having the maximum lattice parameter of 7.36 Å; The lattice parameters of the C-Janus $A_2BCX_3Y_3$ monolayers range from 6.63 to 7.13 Å, where the $Bi_2SiGeSe_3Te_3$ monolayer having the maximum lattice parameter of 7.13 Å. The variation of lattice parameters can be attributed to the size of atomic radius, therefore the structure with the largest atomic radius in each class of Janus has the largest lattice parameter.

TABLE SI. For original and Janus monolayers: lattice constant ($a = b$), band gap without and with SOC ($E_{g\text{-}PBE}$ and $E_{g\text{-}PBE+SOC}$), cohesive energy (E_{coh}), position and constant α_R of Rashba effect (C_1 and V_1 represent the conduction band and valence band closest to the Fermi level, respectively.), dipole moment (P).

Classes	Systems	$a=b$ (Å)	$E_{g\text{-}PBE}$ (eV)	$E_{g\text{-}PBE+SOC}$ (eV)	E_{coh} (eV/atom)	*Position* (Γ)	α_R (eVÅ)	P (e×Å)
$A_2B_2Te_6$	$Sb_2Si_2Te_6$	7.23	1.04(i)	0.90	-3.18	/	0	0
	$Sb_2Ge_2Te_6$	7.29	0.67(i)	0.58	-2.99	/	0	0
	$Bi_2Si_2Te_6$	7.33	1.38(i)	0.83	-3.22	/	0	0
$A_2B_2X_3Y_3$	$Sb_2Ge_2S_3Se_3$	6.68	0.90(i)	0.84	-3.36	C_1/V_1	0.06/0.41	0.089
	$Sb_2Ge_2S_3Te_3$	6.94	1.12(i)	0.99	-3.22	C_1	0.57	0.213
	$Sb_2Ge_2Se_3Te_3$	7.06	0.82(i)	0.75	-3.12	C_1	0.74	0.129
	$Sb_2Si_2S_3Se_3$	6.59	1.33(i)	1.23	-3.65	V_1	0.34	0.093
	$Sb_2Si_2S_3Te_3$	6.87	1.50(i)	1.34	-3.47	C_1	0.49	0.223
	$Sb_2Si_2Se_3Te_3$	6.99	1.20(i)	1.08	-3.34	C_1	0.64	0.134
	$Bi_2Ge_2S_3Se_3$	6.78	1.24(i)	0.96	-3.42	V_1	0.47	0.089
	$Bi_2Ge_2S_3Te_3$	7.04	1.28(d)	0.73	-3.27	C_1	0.15	0.211
	$Bi_2Ge_2Se_3Te_3$	7.15	1.12(i)	0.74	-3.16	C_1	0.34	0.127
	$Bi_2Si_2S_3Se_3$	6.70	1.65(i)	1.22	-3.70	V_1	0.41	0.091
	$Bi_2Si_2S_3Te_3$	6.97	1.76(d)	1.02	-3.52	C_1	0.16	0.218
	$Bi_2Si_2Se_3Te_3$	7.09	1.51(i)	1.02	-3.38	C_1	0.27	0.131
A_2BCX_6	Sb_2SiGeS_6	6.49	1.32(i)	1.27	-3.63	C_1	0.07	0.022
	$Sb_2SiGeSe_6$	6.78	0.94(i)	0.88	-3.38	C_1/V_1	0.11/0.17	0.019
	$Sb_2SiGeTe_6$	7.26	0.88(i)	0.75	-3.08	C_1	0.30	0.013
	Bi_2SiGeS_6	6.60	1.63(i)	1.28	-3.69	C_1	0.14	0.016
	$Bi_2SiGeSe_6$	6.87	1.28(i)	0.97	-3.43	C_1/V_1	0.16/0.30	0.014
	$Bi_2SiGeTe_6$	7.36	1.21(i)	0.73	-3.12	C_1	0.23	0.011
$A_2BCX_3Y_3$	$Sb_2SiGeSe_3S_3$	6.63	1.15(i)	1.07	-3.49	C_1/V_1	0.24/0.25	0.070
	$Sb_2SiGeTe_3S_3$	6.90	1.33(i)	1.19	-3.31	C_1	0.70	0.202
	$Sb_2SiGeS_3Se_3$	6.64	1.14(i)	1.06	-3.52	V_1	0.51	0.111
	$Sb_2SiGeTe_3Se_3$	7.02	1.03(i)	0.93	-3.21	C_1	0.86	0.116
	$Sb_2SiGeS_3Te_3$	6.91	1.33(i)	1.18	-3.37	C_1	0.27	0.237
	$Sb_2SiGeSe_3Te_3$	7.03	1.04(i)	0.93	-3.24	C_1	0.43	0.148

$Bi_2SiGeSe_3S_3$	6.74	1.49(i)	1.13	-3.54	C_1/V_1	0.15/0.28	0.075
$Bi_2SiGeTe_3S_3$	7.00	1.59(d)	0.93	-3.36	C_1	0.43	0.202
$Bi_2SiGeS_3Se_3$	6.75	1.46(i)	1.11	-3.58	C_1/V_1	0.29/0.58	0.105
$Bi_2SiGeTe_3Se_3$	7.12	1.34(i)	0.93	-3.26	C_1	0.58	0.116
$Bi_2SiGeS_3Te_3$	7.01	1.51(d)	0.85	-3.42	/	0	0.227
$Bi_2SiGeSe_3Te_3$	7.13	1.34(i)	0.87	-3.29	/	0	0.142

Band structures of original and Janus monolayers

The band structures of 3 original monolayers and 30 Janus monolayers using PBE method with and without SOC are shown in Fig. S1. When SOC is taken into account, we find that RSS occurs in most Janus monolayers, varying from 0.06 to 0.86 eVÅ. However, for some monolayers, such as $Sb_2Si_2S_3Te_3$, although the RSS also appears at the CBM, it is too weak to be calculated according to the formula, so we do not consider it. In addition, for $Sb_2SiGeSe_6$, $Bi_2SiGeSe_6$, $Sb_2Ge_2S_3Se_3$, $Sb_2Si_2S_3Se_3$, $Bi_2Ge_2S_3Se_3$, $Bi_2Si_2S_3Se_3$, $Sb_2SiGeSe_3S_3$, $Sb_2SiGeS_3Se_3$, $Bi_2SiGeSe_3S_3$ and $Bi_2SiGeS_3Se_3$ monolayers, their first valence band (V_1) exhibits the Rashba effect at the Γ point, but since it is not at the VBM, the conducting holes or electrons will be disturbed by other states near the Fermi level, so we do not further discuss it.

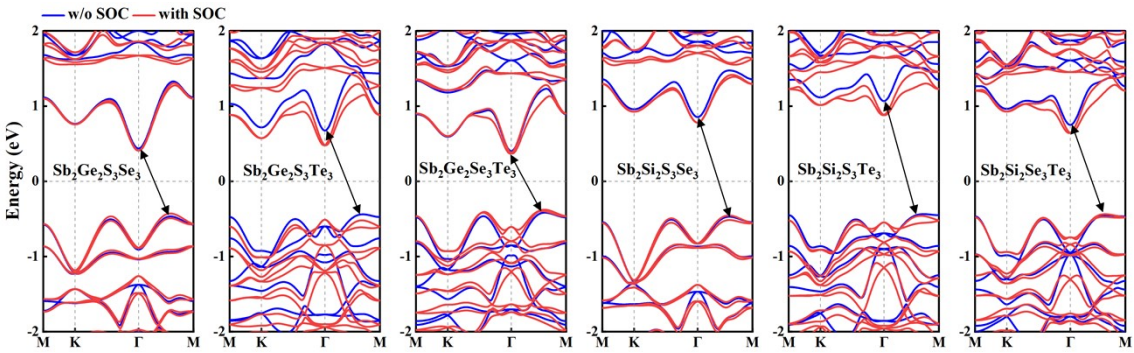

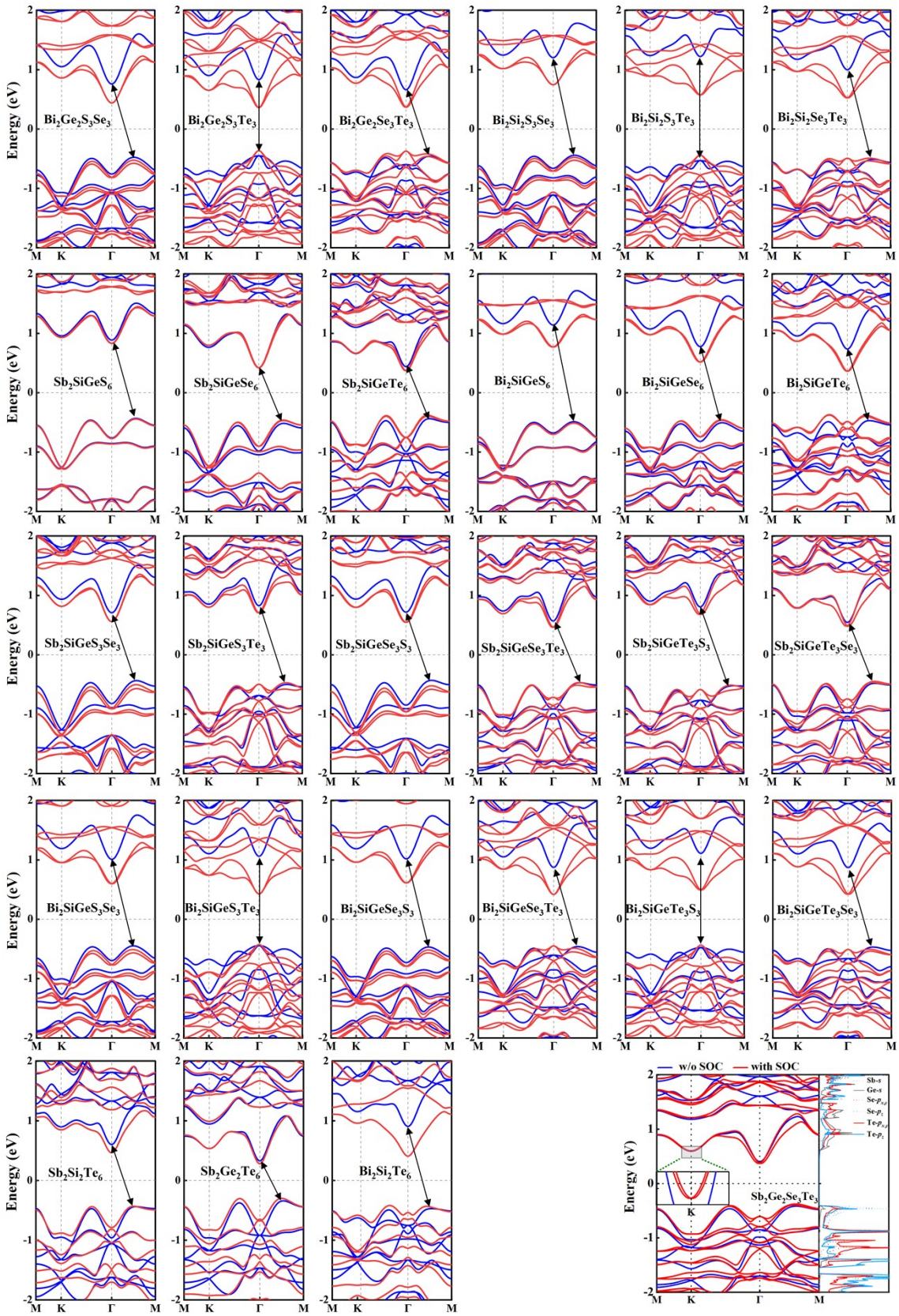

FIG. S1. Band structures of original and Janus monolayers.

Electric field tuning of the Rashba effect

The electric field ranges from -0.3 to 0.3 VÅ^{-1}, which can be achieved in the experiment[1]. The calculated variation of the Rashba constant α_R with the E_{ex} is shown in Fig. S2. We find that α_R is linearly dependent on the E_{ex}. Furthermore, the electric field response rate（$k = \frac{\Delta\alpha_R}{\Delta E}$）has been calculated, whose $|k|$ values are greater than 0.1 eÅ^2.

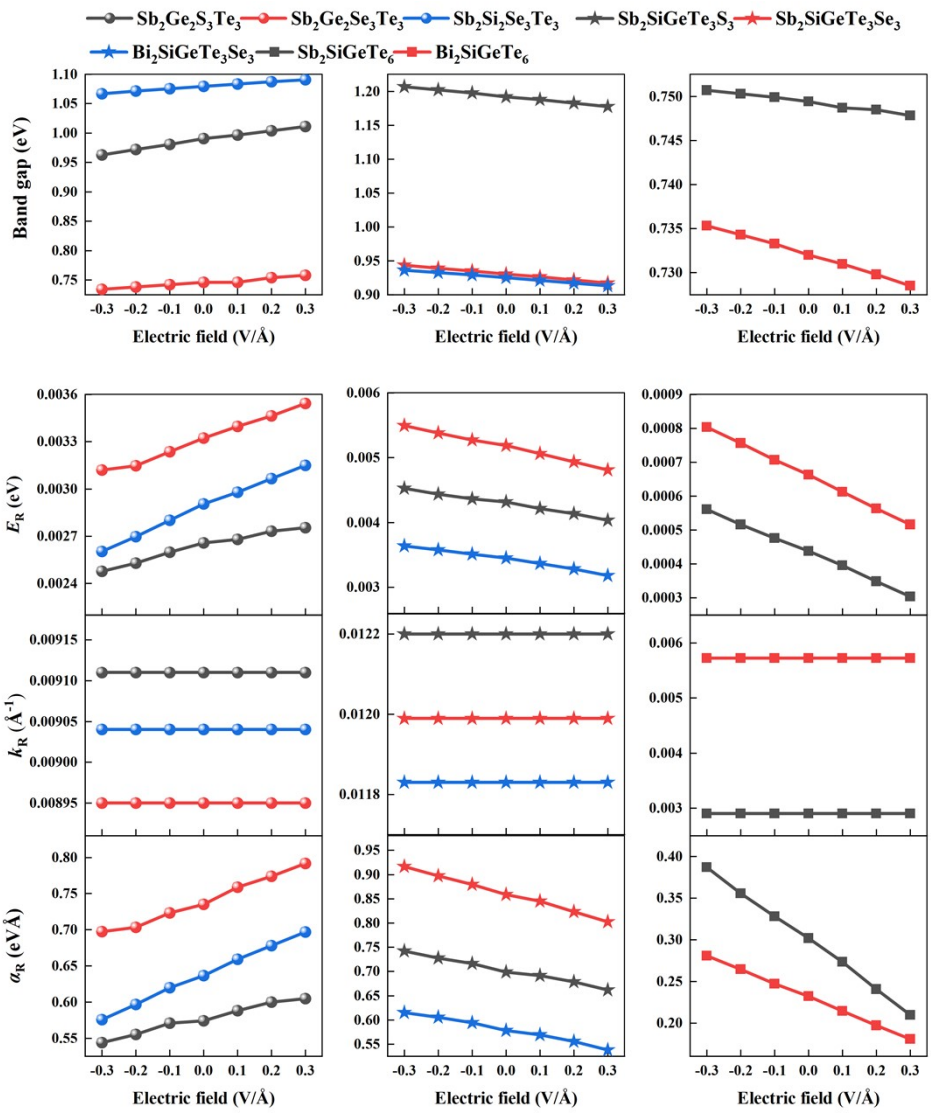

FIG. S2. The band gap, Rashba energy E_R, momentum offset k_R, Rashba constant α_R of T-, I-, and C-Janus monolayers under external electric field (E_{ex}).

Polarization properties of Janus monolayers

Previous studies have shown that the breaking of intrinsic mirror symmetry in Janus 2D materials leads to some fascinating polarization-dependent properties such as different surface work functions, dipole moment, and E_{in}[2,3]. Specifically speaking, the electrostatic potential energy peaks of the original systems are symmetric, consistent with the symmetric crystal structures, as listed in Fig. S3(a_1). However, for the Janus systems with broken structural symmetry, the electrostatic potential distributions are asymmetrical with different peaks in the different positions, which leads to different work functions at X and Y atomic surfaces [Fig. S3(a_2)]. Moreover, we further investigate the mirror symmetry breaking induced dipole moment to confirm the polarization effect (Table SI). The work function difference $\Delta\Phi$ between both surfaces is directly affected by the dipole moment P, which is in agreement with the Helmholtz equation. Considering that the vertical intrinsic electric field E_{in} is generally the key factor affecting the α_R of Janus Rashba systems and even its modulation trend under E_{ex}, which could be directly reflected in aspects of work function and electrostatic potential, dipole moment, or charge transfer, we have carried out analysis on the above physical quantities (Fig. S4-S7).

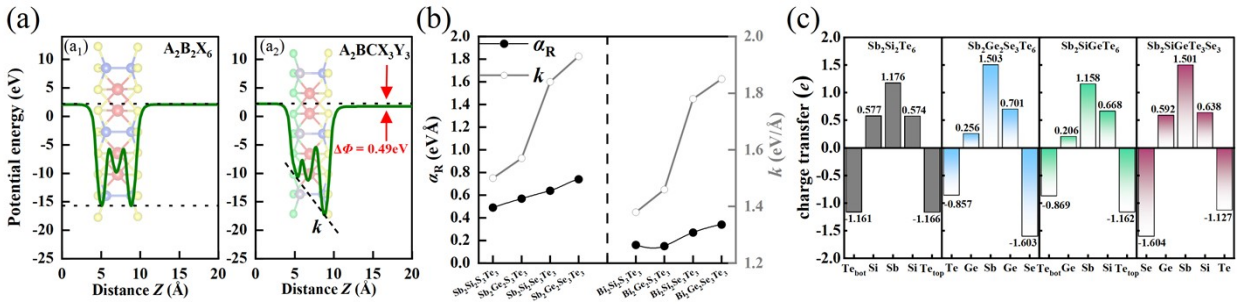

FIG. S3. (a) Planar average of the electrostatic potential of (a_1) original and (a_2) Janus monolayers along the z direction (taking the original $Sb_2Ge_2Te_6$ and composite Janus $Sb_2SiGeTe_3Se_3$ monolayer as examples). (b) The electrostatic potential slope k on both sides and Rashba constant α_R for the T-Janus $A_2B_2X_3Y_3$ monolayers. (c) Charge transfer of $Sb_2Si_2Te_6$, $Sb_2Ge_2Se_3Te_3$, $Sb_2SiGeTe_6$, and $Sb_2SiGeTe_3Se_3$ monolayers.

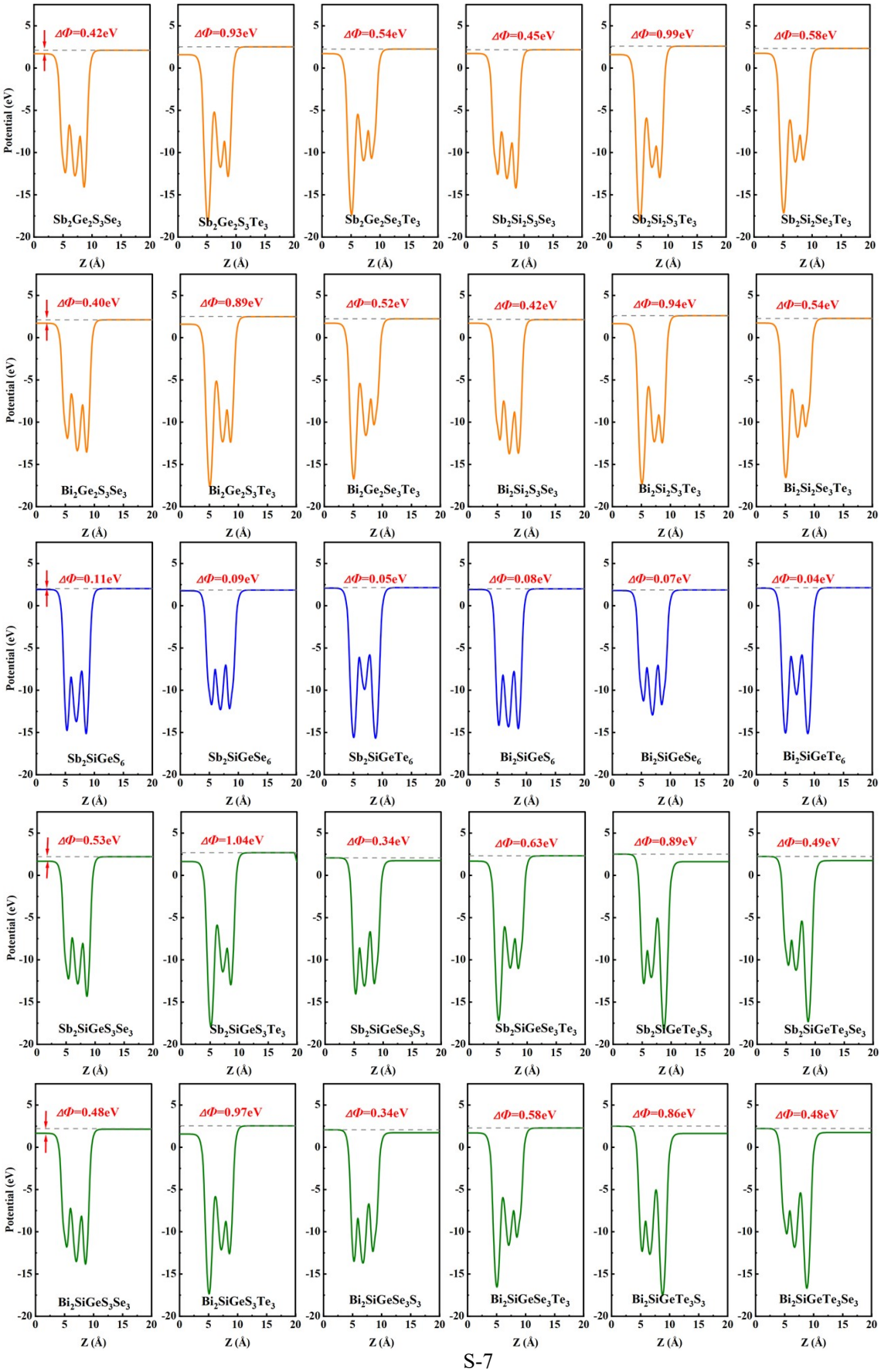
ΔΦ=0.42eV
Sb2Ge2S3Se3
ΔΦ=0.93eV
Sb2Ge2S3Te3
ΔΦ=0.54eV
Sb2Ge2Se3Te3
ΔΦ=0.45eV
Sb2Si2S3Se3
ΔΦ=0.99eV
Sb2Si2S3Te3
ΔΦ=0.58eV
Sb2Si2Se3Te3
ΔΦ=0.40eV
Bi2Ge2S3Se3
ΔΦ=0.89eV
Bi2Ge2S3Te3
ΔΦ=0.52eV
Bi2Ge2Se3Te3
ΔΦ=0.42eV
Bi2Si2S3Se3
ΔΦ=0.94eV
Bi2Si2S3Te3
ΔΦ=0.54eV
Bi2Si2Se3Te3
ΔΦ=0.11eV
Sb2SiGeS6
ΔΦ=0.09eV
Sb2SiGeSe6
ΔΦ=0.05eV
Sb2SiGeTe6
ΔΦ=0.08eV
Bi2SiGeS6
ΔΦ=0.07eV
Bi2SiGeSe6
ΔΦ=0.04eV
Bi2SiGeTe6
ΔΦ=0.53eV
Sb2SiGeS3Se3
ΔΦ=1.04eV
Sb2SiGeS3Te3
ΔΦ=0.34eV
Sb2SiGeSe3S3
ΔΦ=0.63eV
Sb2SiGeSe3Te3
ΔΦ=0.89eV
Sb2SiGeTe3S3
ΔΦ=0.49eV
Sb2SiGeTe3Se3
ΔΦ=0.48eV
Bi2SiGeS3Se3
ΔΦ=0.97eV
Bi2SiGeS3Te3
ΔΦ=0.34eV
Bi2SiGeSe3S3
ΔΦ=0.58eV
Bi2SiGeSe3Te3
ΔΦ=0.86eV
Bi2SiGeTe3S3
ΔΦ=0.48eV
Bi2SiGeTe3Se3
Potential (eV)
Z (Å)

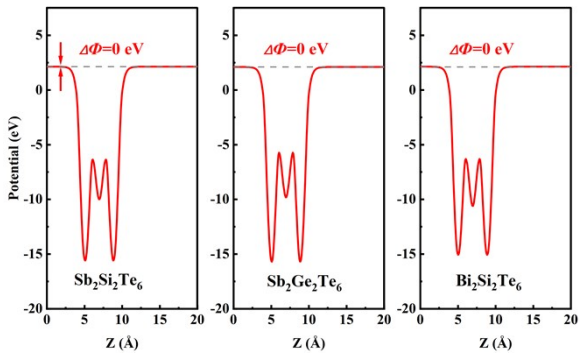

FIG. S4. Planar average of the electrostatic potential of Janus and original monolayers along the *z* direction. The yellow, blue, green and red solid lines indicate the configurations of T-, I-, C-Janus monolayers and original monolayers, respectively.

The electric field can be estimated by the "slope *k*" of the potential energy diagram:

$$k = \frac{V(X) - V(Y)}{d(X) - d(Y)}$$

where *V(X/Y)* is the vertical planar average potential on X/Y atom, *d(X/Y)* is the distance between origin and X/Y atom, as shown in Fig. S5.

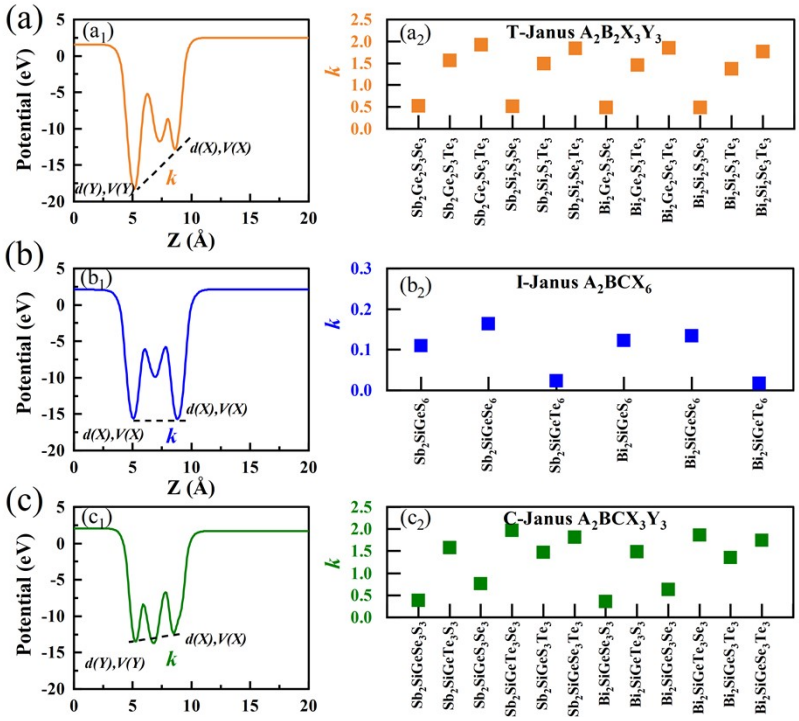

FIG. S5. Slope of potential energy differences for three classes of Janus structures (a) T-Janus $A_2B_2X_3Y_3$,(b) I-Janus A_2BCX_6 and (c) C-Janus $A_2BCX_3Y_3$.

For T-Janus, due to its characteristic of having only the outer-layer elements differing, T-Janus $A_2B_2X_3Y_3$ exhibits a distinct work function difference ΔΦ and the slope of potential energy difference k [Fig. S6(a)]. According to the Helmholtz relation, the work function difference ΔΦ is positively correlated with the dipole moment P, thus T-Janus possesses a significant dipole moment. However, as observed from the locally magnified potential energy diagrams in Fig. S6(b) and S6(c), there is no significant difference in work function, potential energy between I-Janus A_2BCX_6 and C-Janus $A_2BCX_3Y_3$. Similarly, both have smaller dipole moments. In particular, for I-Janus A_2BCX_6, where the atoms at both ends are identical, the work function and potential energy difference are nearly zero. The method of measuring the E_{in} through Bader charge transfer analysis is not limited by the type of Janus configuration. In addition, using charge transfer to unify the description can well reflect the changes in local electric fields in subsequent single atom adsorption.

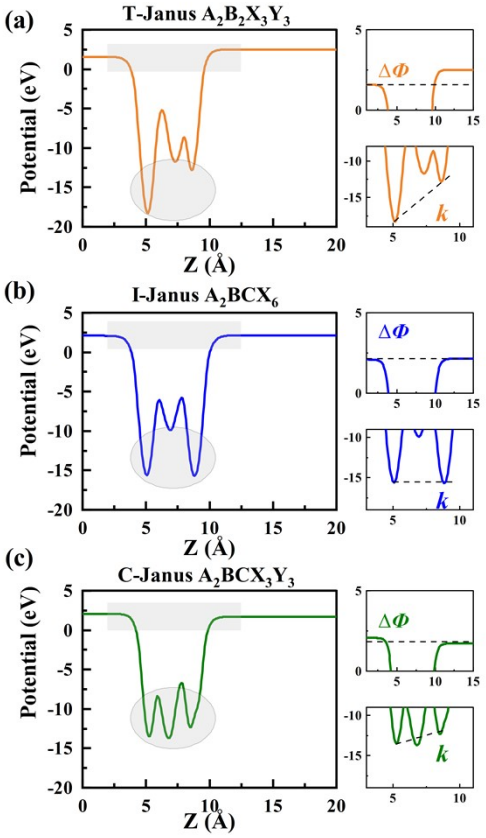

FIG. S6. Images of the local magnified work function difference as well as the slope k of the potential energy difference for three classes of Janus structures (a) T-Janus $A_2B_2X_3Y_3$, (b) I-Janus A_2BCX_6 and (c) C-Janus $A_2BCX_3Y_3$.

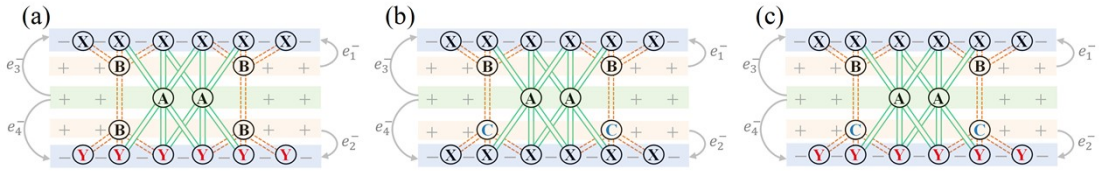

FIG. S7. Schematic illustrations of charge transfer in the (a) T-Janus, (b) I-Janus, and (c)

C-Janus structures. $e_1^-, e_2^-, e_3^-, e_4^-$ represent the flow of electrons between different layers.

$$Q_d = \left| e_1^- + e_3^- - e_2^- - e_4^- \right|$$

$$Q_t = \left| e_1^- + e_2^- + e_3^- + e_4^- \right|$$

	Q_Y	Q_B	Q_A	Q_B	Q_X	Q_d	Q_t
$Sb_2Ge_2S_3Se_3$	1.579	-0.658	-2.069	-0.948	2.096	0.517	3.675
$Sb_2Ge_2S_3Te_3$	0.841	-0.304	-1.749	-0.907	2.119	1.278	2.96
$Sb_2Ge_2Se_3Te_3$	0.857	-0.256	-1.503	-0.701	1.603	0.746	2.46
$Sb_2Si_2S_3Se_3$	2.265	-1.264	-2.083	-1.855	2.938	0.673	5.203
$Sb_2Si_2S_3Te_3$	1.163	-0.508	-1.740	-1.865	2.950	1.787	4.113
$Sb_2Si_2Se_3Te_3$	1.147	-0.585	-1.494	-1.354	2.286	1.139	3.433
$Bi_2Ge_2S_3Se_3$	1.638	-0.660	-2.175	-0.953	2.149	0.511	3.787
$Bi_2Ge_2S_3Te_3$	0.945	-0.311	-1.897	-0.916	2.178	1.233	3.123
$Bi_2Ge_2Se_3Te_3$	0.957	-0.257	-1.671	-0.703	1.674	0.717	2.631
$Bi_2Si_2S_3Se_3$	2.333	-1.278	-2.187	-1.863	2.994	0.661	5.327
$Bi_2Si_2S_3Te_3$	1.249	-0.507	-1.886	-1.879	3.023	1.774	4.272
$Bi_2Si_2Se_3Te_3$	1.256	-0.580	-1.680	-1.362	2.366	1.11	3.622

TABLE SII. The charge transfer of atoms in T-Janus $A_2B_2X_3Y_3$ monolayer. Q_A ($e_3^- + e_4^-$), Q_B ($e_1^- + e_2^-$), Q_X ($e_1^- + e_3^-$) and Q_Y ($e_2^- + e_4^-$) represent the charge transfer amount of each layer respectively. Negative values represent electron loss of corresponding

	Q_X	Q_C	Q_A	Q_B	Q_X	Q_d	Q_t
Sb_2SiGeS_6	2.101	-0.763	-2.309	-1.998	2.970	0.869	5.071
$Sb_2SiGeSe_6$	1.594	-0.502	-1.840	-1.554	2.303	0.709	3.897
$Sb_2SiGeTe_6$	0.869	-0.206	-1.158	-0.668	1.162	0.293	2.031
Bi_2SiGeS_6	2.126	-0.761	-2.387	-1.995	3.016	0.89	5.142
$Bi_2SiGeSe_6$	1.646	-0.502	-1.964	-1.549	2.369	0.723	4.015
$Bi_2SiGeTe_6$	0.993	-0.212	-1.377	-0.687	1.283	0.29	2.276

	Y	C	A	B	X	Q_d	Q_t
$Sb_2SiGeSe_3S_3$	2.100	-0.767	-2.086	-1.541	2.293	0.193	4.393
$Sb_2SiGeTe_3S_3$	2.119	-0.859	-1.766	-0.609	1.116	1.003	3.235
$Sb_2SiGeS_3Se_3$	1.578	-0.496	-2.057	-1.999	2.975	1.397	4.553
$Sb_2SiGeTe_3Se_3$	1.604	-0.592	-1.501	-0.638	1.127	0.477	2.731
$Sb_2SiGeS_3Te_3$	0.855	-0.107	-1.716	-2.003	2.970	2.115	3.825
$Sb_2SiGeSe_3Te_3$	0.867	-0.186	-1.494	-1.493	2.306	1.439	3.173
$Bi_2SiGeSe_3S_3$	2.146	-0.774	-2.188	-1.551	2.367	0.221	4.513
$Bi_2SiGeTe_3S_3$	2.171	-0.867	-1.907	-0.645	1.248	0.923	3.419
$Bi_2SiGeS_3Se_3$	1.644	-0.497	-2.175	-2.005	3.033	1.389	4.677
$Bi_2SiGeTe_3Se_3$	1.675	-0.596	-1.688	-0.649	1.258	0.417	2.933
$Bi_2SiGeS_3Te_3$	0.953	-0.110	-1.875	-2.021	3.053	2.1	4.006

TABLE SIII. The charge transfer of atoms in I-Janus A_2BCX_6 monolayer.

TABLE SIV. The charge transfer of atoms in C-Janus $A_2BCX_3Y_3$ monolayer.

In pristine $A_2B_2X_6$, there is no difference in electronegativity between the atoms on both sides of the center, which results in a charge transfer difference Q_d of 0 and the absence of E_{in}. For the Janus $A_2B_2X_3Y_3$, due to the difference in electronegativity between the upper and lower atomic layers, there will be a non-zero Q_d and E_{in}. The schematic diagram of the Janus structures (e.g., T-Janus structure) and the charge transfer model are shown in Fig.S8(a). When applying an E_{ex}, the charge transfer Q_d ($Q_d = |e^-_1 + e^-_3 - e^-_2 - e^-_4|$) and Q_t ($Q_t = |e^-_1 + e^-_2 + e^-_3 + e^-_4|$) combined with its response to the E_{ex} ($k_1 = \frac{\Delta Q_d}{\Delta E}$ and $k_2 = \frac{\Delta Q_t}{\Delta E}$), we establish a rough relationship between charge transfer Q_{d+t} (defined as $Q_{d+t} = Q_d \times k_1 + Q_t \times k_2$) and α_R. When Q_{d+t} is greater than 0, the α_R enhances (weakens) monotonically with the increase of E_p (E_n) strength; When Q_{d+t} is less than 0, the α_R weakens (enhances) monotonically with the increase of E_p (E_n) strength.

The Fig. S8(c) and Fig. S8(d) illustrates the linear variation of Q_d and Q_t under E_{ex}, we define their electric field responses as $k_1 = \frac{\Delta Q_d}{\Delta E}$ and $k_2 = \frac{\Delta Q_t}{\Delta E}$, respectively. Considering that Q_d can reflect the strength of E_{in} by generating a potential gradient in the basal plane at both ends of monolayers, Q_t reflects the strength of the electronegativity difference between atoms by the total amount of charge transfer. To explain the change in α_R of Janus structures under the action of E_{ex}, we continue to use the mathematical expression $Q_d \times k_1 + Q_t \times k_2$ based on Q_d and Q_t, which is abbreviated as Q_{d+t^4} .

For the charge transfer of T-Janus structures under E_{ex}, we obtain the relationship between $\frac{\Delta \alpha_R}{\Delta E}$ and Q_{d+t} and extend it to I- and C-Janus structures [Fig. S8(e)]. As a result, the numerical values of Q_{d+t} are 0.34, 0.26 and 0.46 for SGST-1, SGST-2 and SSST monolayers; The C-Janus structures SSGTS-1, SSGTS-2, BSGTS, and I-Janus structures SSGT, BSGT have values of -1.03, -0.86, -0.93, -0.42 and -0.39, respectively (Table SV).

Therefore, when combining the Q_d with another Q_t related to element electronegativity, the trend of α_R increasing or decreasing with the strength of E_{ex} can be further approximately confirmed based

	Q_d	k_1	Q_t	k_2	Q_{d+t}

on the slope of charge transfer change under E_{ex}.

TABLE SV. The data associated with Q_{d+t} comprises Q_d, k_1, Q_t, and k_2, where k_1 and k_2 denote the electric field rate of change for Q_d and Q_t, respectively.

$Sb_2Si_2Se_3Te_3$	1.139	0.43	3.433	-0.01	0.46
$Sb_2SiGeTe_3S_3$	1.003	-0.41	3.235	-0.19	-1.03
$Sb_2SiGeTe_3Se$	0.477	-0.44	2.731	-0.23	-0.86
3					
$Bi_2SiGeTe_3Se_3$	0.417	-0.45	2.933	-0.25	-0.93
$Sb_2SiGeTe_6$	0.293	0.50	2.031	-0.28	-0.42
$Bi_2SiGeTe_6$	0.29	0.52	2.276	-0.24	-0.39

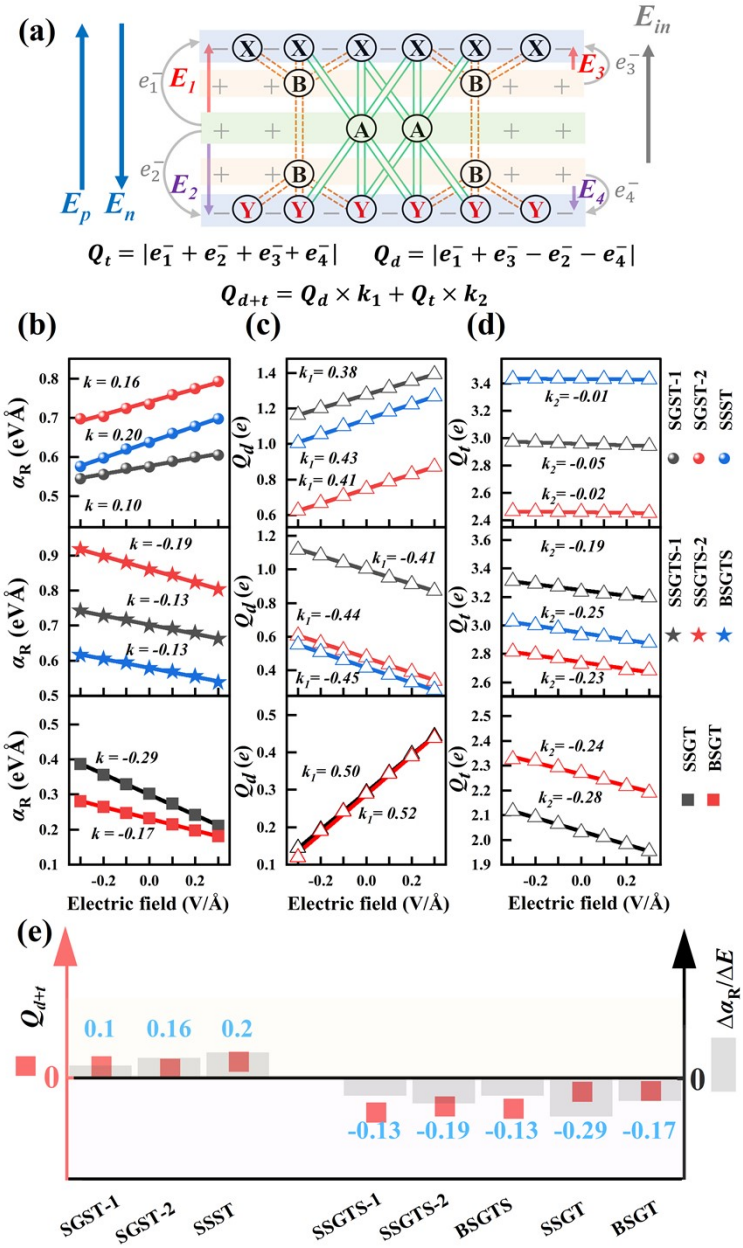

FIG. S8. (a) Schematic diagram of charge transfer of T-Janus $A_2B_2X_3Y_3$. $e_1^-, e_2^-, e_3^-, e_4^-$ represent the flow of electrons between different layers. E_1, E_2, E_3, E_4 represent the localized electric field. The gray and blue arrows represent E_{in} and E_{ex}, respectively, where the positive electric field (E_p) along the z-direction, and the negative electric field in the opposite direction (E_n). Under an external electric field (b) α_R response is quantified by parameter k, (c) Q_d response is governed by parameter k_1

Atomic adsorption reconfigures charge transfer

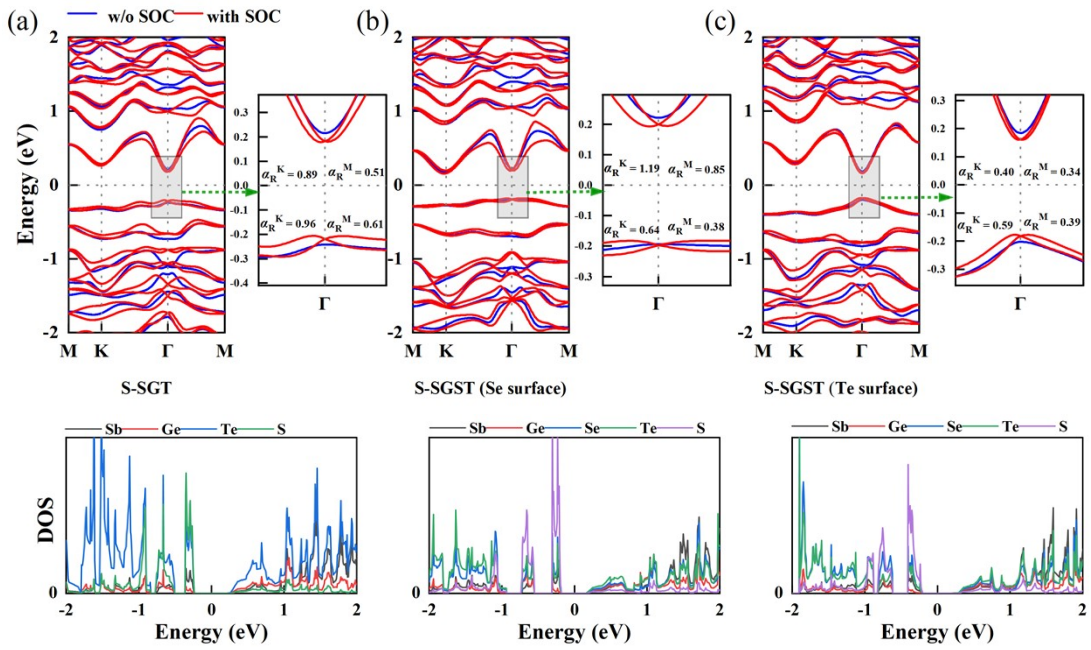

FIG. S9. (a) Band structures and DOS of S adsorbed on SGT. Band structures and DOS of (b) S adsorbed on SGST (Se-surface), and (c) S adsorbed on SGST (Te-surface).

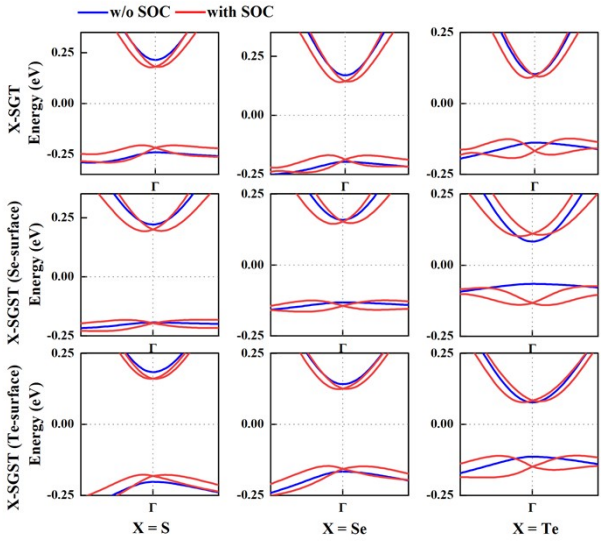

FIG. S10. Band structures of X-SGT and X-SGST systems. Blue and red solid lines indicate methods of PBE and PBE+SOC, respectively.

BN/SGST and BN/S-SGST heterostructures

In experiments, 2D materials are usually grown on a substrate, and the electronic properties are affected by the substrate. Generally, the insulating substrate materials used for 2D devices are BN, AlN, and GaN. The lattice mismatches for SGST/BN (3×3×1), SGST/AlN (2×2×1), and SGST/GaN (2×2×1) are 6%, 12%, and 9%, respectively. Considering practical feasibility and minimizing lattice mismatch between the two stacks, we construct the heterostructure using a 3×3×1 supercell of BN and one SGST layer and investigate their electronic properties. Electronic structure calculations show that heterostructures retain the indirect or direct band gap characteristics of their original systems, but the band gap is significantly reduced compared to the original systems. The band gap of the BN/SGST heterostructures decreases to 0.47 eV (Se-surface) and 0.46 eV (Te-surface), and the band gap of the BN/S-SGST heterostructures decreases to 0.05 eV (Se-surface) and 0.03 eV (Te-surface). When SOC is taken into account, the band gap of the BN/SGST heterostructures decreases to 0.42 eV, 0.41 eV, and the band gap of the BN/S-SGST heterostructures decreases to 0.05 eV, 0.05 eV. It is worth noting that for the BN/S-SGST system, significant RSS occurs simultaneously at CBM and VBM, which can be attributed to the presence of Te and Se atomic orbitals at CBM and S atomic orbital at VBM, as shown in the projected DOS diagrams of the two heterostructures [Fig. S11(b)].

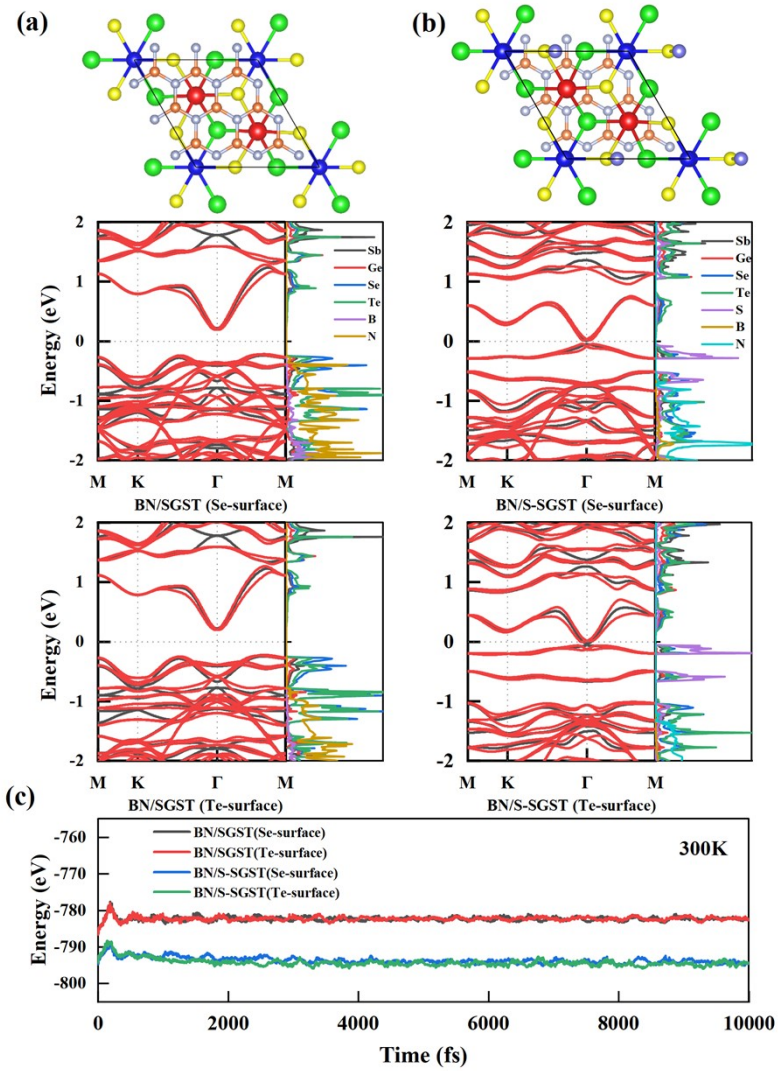

FIG. S11. (a) Band structures and DOS of BN/SGST heterostructures (Se-surface and Te-surface) (b) Band structures and DOS of BN/S-SGST (Se-surface and Te-surface) heterostructures. (c) AIMD simulations of total energy fluctuation under 10 ps at 300K of BN/SGST and BN/S-SGST heterostructures.

References

1. Domaretskiy, D. *et al.* Quenching the bandgap of two-dimensional semiconductors with a perpendicular electric field. *Nat. Nanotechnol.* **17**, 1078–1083 (2022).
2. Ghobadi, N., Gholami Rudi, S. & Soleimani-Amiri, S. Electronic, spintronic, and piezoelectric properties of new Janus Zn A X Y (A = Si , Ge , Sn , and X , Y = S , Se , Te) monolayers. *Phys. Rev. B* **107**, 075443 (2023).
3. Liu, M.-Y., Gong, L., He, Y. & Cao, C. Tuning Rashba effect, band inversion, and spin-charge conversion of Janus X Sn 2 Y monolayers via an external field. *Phys. Rev. B* **103**, 075421 (2021).
4. Tian, Q. *et al.* Inverse Janus design of two-dimensional Rashba semiconductors. *Phys. Rev. B* **108**,

115130 (2023).